## 2.7 Wake Field and Beam Coupling Impedance Simulations

Uwe Niedermayer and Erion Gjonaj
Institut für Theorie elektromagnetischer Felder,
Technische Universität Darmstadt
Schlossgartenstr. 8, 64289 Darmstadt, Germany
Mail to: niedermayer@temf.tu-darmstadt.de

### 2.7.1 Introduction

Wake potentials and beam coupling impedances can be calculated analytically only if the structures are fairly simple and an appropriate coordinate system can be attached. In practice this is often not the case and one has to rely on numerical techniques. Although the term beam coupling impedance was introduced first in the Frequency Domain (FD) by Vaccaro [1] in 1966, first numerical wake field computations were performed in the Time Domain (TD) by Balakin et al. [2] in 1978, and Weiland [3] in 1980. Nowadays, TD methods on structured meshes are the most common way to determine beam coupling impedances; they are available in many commercial and non-commercial codes.

Explicit TD methods require only matrix-vector multiplications for time stepping, which makes them computationally efficient. Usually they are based on Finite Differences Time Domain (FDTD [4]) or Finite Integration Technique (FIT [5]), which result in a coinciding space discretization on a Cartesian mesh. However, in general, mesh and method are independent. For example FIT or the Finite Element Method (FEM) can be applied on tetrahedral, hexahedral, or even mixed meshes.

In explicit TD simulations stability requires fulfilling the Courant Friedrichs Lewy (CFL) condition [6]. This makes them well suited for wave-propagation dominated problems but not well suited for structure-dominated problems, particularly at Low Frequency (LF). The small time step, which is tied to the space step by the CFL condition leads to a massive oversampling of an LF wave. Moreover, sub-relativistic beams and dispersive materials are difficult to treat in TD.

In these rather exotic cases, it makes sense to compute the beam coupling impedance directly in FD. Such computations are somewhat oriented on analytical methods [7], but generalized to arbitrary geometries by discretization methods as FIT or FEM. The current status of FD methods, however, is not as advanced as for TD methods. In particular, there is no high performance tool to compute beam coupling impedance in FD for three-dimensional structures.

In this paper, we will first discuss relevant assumptions and requirements for the computation of wake potentials and impedances in TD and FD. Then we give an overview of methods and codes. In the end, we give two examples; one is a three-dimensional RF-finger bellow structure planned to be used in the LHC which we address in TD and the other is a scenario for FCC-hh beam pipe addressed by a two-dimensional FD approach.

### 2.7.2 Definitions and Assumptions for the Computation of Wakefields and Impedances

The definition of wake potentials decouples the electromagnetical and the mechanical problems in beam dynamics by making the two assumptions:

- Rigid beam approximation: all particles move through the structure with constant velocity,
- Kick approximation: the force continuously acting on the trailing charge is lumped to a single kick (instantaneous change of momentum) after the passage through the structure.

The three-dimensional wake function is generally defined as (see e.g. [8])

$$\vec{W}(\vec{r}_1,\vec{r}_2,s)=\frac{1}{q}\int_{-\infty}^{\infty}[\vec{E}+\vec{v}\times\vec{B}](\vec{r}_2,z_2,t=(s+z)/v)dz_2\,, \tag{1}$$

where $\vec{r}_1,\vec{r}_2$ are the transverse coordinates of the leading and trailing charge, respectively. Equation 1 fulfills the Panofsky-Wenzel (PW) theorem [9] as $\nabla'\times\vec{W}(\vec{r}_1,\vec{r}_2,s)=0,$ where the relative gradient is $\nabla'=(\partial_{x2},\partial_{y2},-\partial_s)^T$. A supplement to the PW theorem is the fact that the longitudinal wake function is a harmonic function of the transverse coordinates in the ultra-relativistic limit. This is the basis of several methods to modify the wake integration contour [10,11]. Among the most famous ones are the indirect test beam method [12] and the indirect interfaces [13] method. An approach to avoid lengthy wake integration for evanescent waveguide modes in the beam pipe after a cavity is presented in [14]. Finally, generalized methods for arbitrary structures are discussed in an abstract mathematical framework in [15].

The improper integral (1) exists only if the assumed infinite beam pipe connections do not cause any wakefields, i.e. the following conditions have to be fulfilled:

- smooth pipe (no geometric wake fields),
- perfectly conducting pipe (no resistive wake fields),
- ultra-relativistic beam (no space-charge wake fields).

Note that the last two requirements can be relaxed by taking into account a pipe stub impedance per unit length. However inserting a nonrelativistic beam into a 3D structure is involved and requires a numerical Lorentz transformation [16].

The wake potential is connected to the wake function by convolution with the bunch profile (line density $\lambda(s)$),

$$W_{pot}(s)=\int_{-\infty}^{\infty}W(s')\lambda(s-s')ds'\,. \tag{2}$$

Due to the minimal duration–bandwidth product, a Gaussian bunch

$$\lambda(z,t)=\frac{q}{\sqrt{2\pi}\sigma_s}\exp(0.5(z-vt)^2/\sigma_s^2) \tag{3}$$

is usually employed for the excitation. Fourier transform over s = vt-z leads to

$$|\lambda(\omega)|=\frac{q}{v}\exp(0.5\omega^2/\sigma_\omega^2)\quad,\quad \sigma_\omega=v/\sigma_s\,. \tag{4}$$

Note that the excitation bunch length $\sigma_s$ in a TD simulation does not necessarily correspond to the true bunch length in the operated accelerator, but rather to the frequency of interest. The point charge impedance is recovered by applying the convolution theorem as

$$Z(\omega) = \frac{1}{\lambda(\omega)} \int_{-\infty}^{\infty} W_{pot}(s) \exp(-i\omega s / v) ds \,. \tag{5}$$

For ultra-relativistic beams the dipolar and quadrupolar transverse impedances can be obtained by displacing the source bunch or the wake integration line, respectively. If the displacement is small, the impedance scales linearly with it and thus one defines a transverse dipolar or quadrupolar impedance in units of Ohms/m, which is obtained from the wake potential in the same way as the longitudinal impedance.

The beam coupling impedance can also be defined directly in FD by the power loss integral of a beam with finite transverse size as

$$Z(\omega) = -\frac{1}{q^2} \int_{beam} \underline{\vec{E}} \cdot \underline{\vec{J}}^* \, dV \,, \tag{6}$$

where $\underline{\vec{J}}, \underline{\vec{E}}$ are the beam current density and the electric field spectral densities, respectively. The dipolar transverse impedance can be obtained accordingly by using a dipolar excitation current density and the PW theorem. Note that the representation of the impedance by a volume integral over the longitudinal electric field and the current density is particularly convenient for the computation on a mesh since discretization noise is averaged out. Moreover, it allows for consistent computation of the space charge impedance in the case of v < c [17].

### 2.7.3 **Time Domain Simulation Tools and Methods**

Computational loads in wake field computation can be heavy, thus parallel codes lead to a significant progress. Nowadays, more than 1e9 mesh cells are easily handled in parallel codes on cluster computers, while on a single machine the limit is at about 1e7 to 1e8. Moreover, an important recent improvement was the introduction of boundary conformal meshing, increasing the convergence order and avoiding extremely fine meshes to approximate the geometry accurately.

For the computation of short range wakes, it is advantageous to use a moving window, i.e. a mesh which moves along with the bunch and re-discretizes the geometry in every time step. The moving mesh approach was first introduced by Bane and Weiland [18] and is nowadays implemented in many codes such as PBCI [19] or GdfidL [20]. For long-range wakes, however, where the desired wake length is much longer than the structure, the moving mesh is rather inappropriate, since the entire wake length needs to be meshed.

Another important property for short-range wake computation in TD is the suppression of numerical dispersion in direction of beam propagation. This can be achieved by e.g. longitudinal-transversal-splitting [19] or TE-TM-splitting [21]. An overview of different TD codes can be found in [22], where these properties are discussed in more detail.

### 2.7.4 **Flexible RF-Finger Structures**

We investigate the structure shown in Fig. 1, which is designed to serve as a shielding for the LHC triplet bellows in point 1 and point 5. The fingers are made from a single copper beryllium sheet of 0.1 mm thickness. In total, it is considered to have 32 such structures in the LHC [23]. The beam coupling impedance is computed using the commercial CST Particle Studio (PS) [24] wake field solver and the PBCI code. The latter is a dedicated

dispersion free, moving window, parallel wake field solver developed at TEMF, TU Darmstadt. Recently, also conformal meshing was added to PBCI.

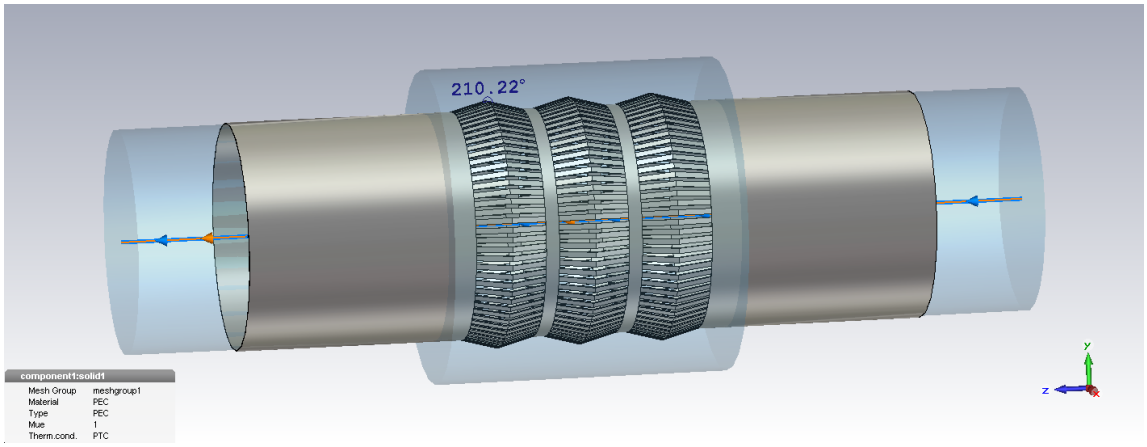


**Figure 1**: RF-Finger and bellow structure.

Since the structure is symmetric with respect to both the x-z and y-z planes, only one quarter of the geometry needs to be modeled when the beam is on axis (see Fig. 2) and only half needs to be modeled for dipolar excitation. When wakefield integration by means of indirect interfaces (see also [13]) is applied, the beam pipe stubs can be chosen to be very short, which reduces the number of cells in the structured mesh significantly. Wave guide port boundaries taking into account at least 50 modes guarantee that the reflections at the beam entry and exit are small. The excitation is applied as a Gaussian bunch with $\sigma_s = 12$ mm.

The simulated wake potential is displayed in Fig. 3, where the different parameters for the PBCI runs are given in Table 1. Figure 4 shows the real and imaginary parts of the impedance obtained by CST PS, where long wake lengths can be easily realized. Finally, Fig. 5 shows a comparison of CST and PBCI impedance magnitude, also for the structure fingers closed, such that only a bellow structure remains. This can be simulated much easier, and the results show good agreement with the simulation of the original structure. From this, one can conclude that the structure works as it should, i.e. shielding the beam from the outside in the frequency range of the beam spectrum. The expected cutoff at which significant field transmission occurs is at f=c/2d=60GHz, where d=2.5mm is the gap between two fingers. Finally, Fig. 6 shows the transverse impedance that also behaves almost identically in both the finger and closed cases.

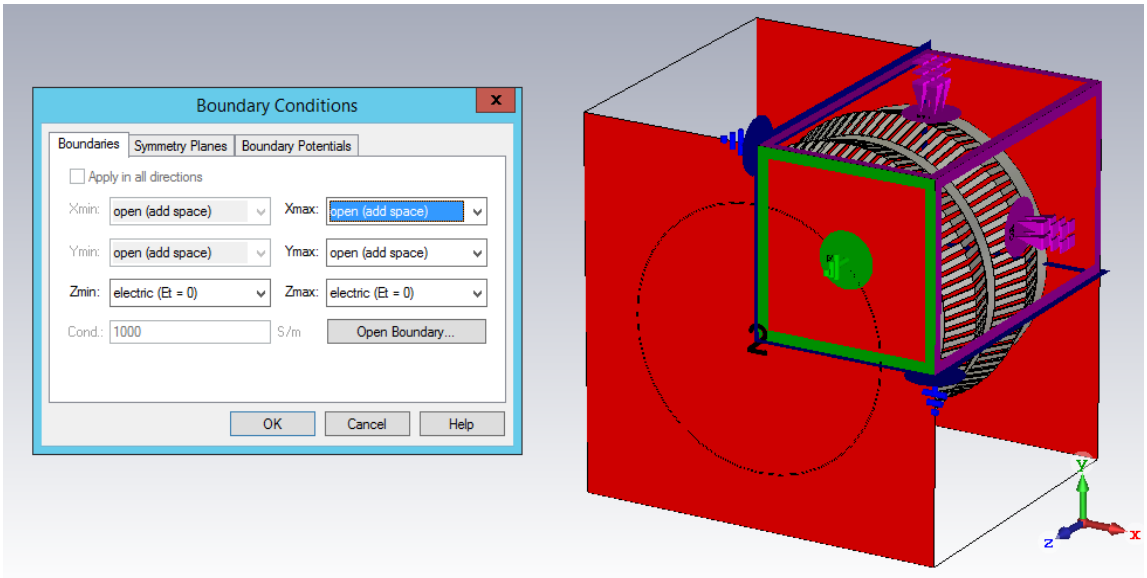


**Figure 2**: Boundary and symmetry conditions.

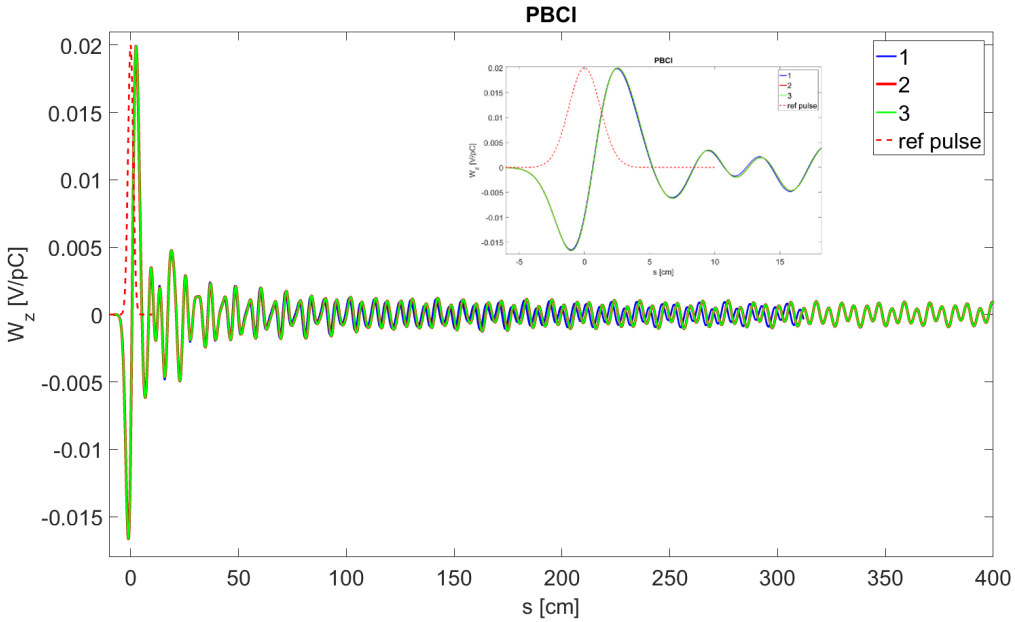


**Figure 3**: Longitudinal wake potential.

**Table 1**: Parameters of PBCI simulation runs.

| | #cells | Wake length | Processes |
|---|---|---|---|
| PBCI1 | 8.6e7 | 3.2m | 83 |
| PBCI2 | 5e8 | 6.4m | 332 |
| PBCI3 | 1e9 | 12.8m | 162 |

We interpret the impedance curves in Figs. 5 and 6 as follows: the first resonance at 5.1 GHz (3.6 GHz for the dipolar impedance) corresponds to a cavity mode. In the absence of losses its quality factor tends to infinity. In the simulations the height of the peak is

limited by the finite wake length and thus increases with increasing wake length. The second peak at 7.8 GHz (6.3 GHz for the dipolar impedance) is independent of the wake length. This is a broadband resonance caused by leaky cavity modes, i.e. cavity modes, which decay due to losses through the pipe. The small peak at 2.28 GHz (1.73 GHz for the dipolar impedance) corresponds to the cutoff of the first TM (TE) waveguide mode.

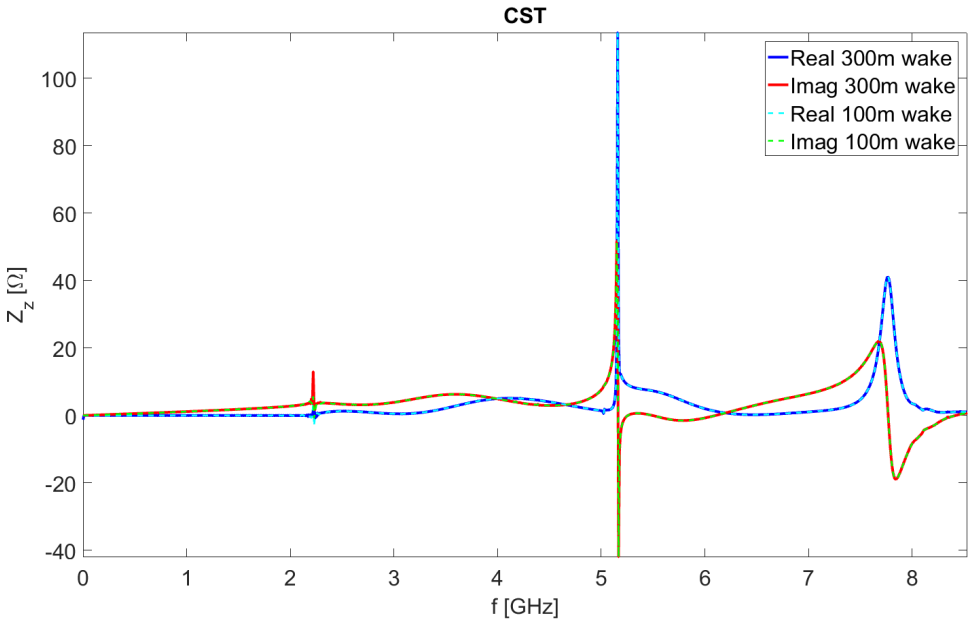


**Figure 4:** Real and imaginary part for different wake lengths.

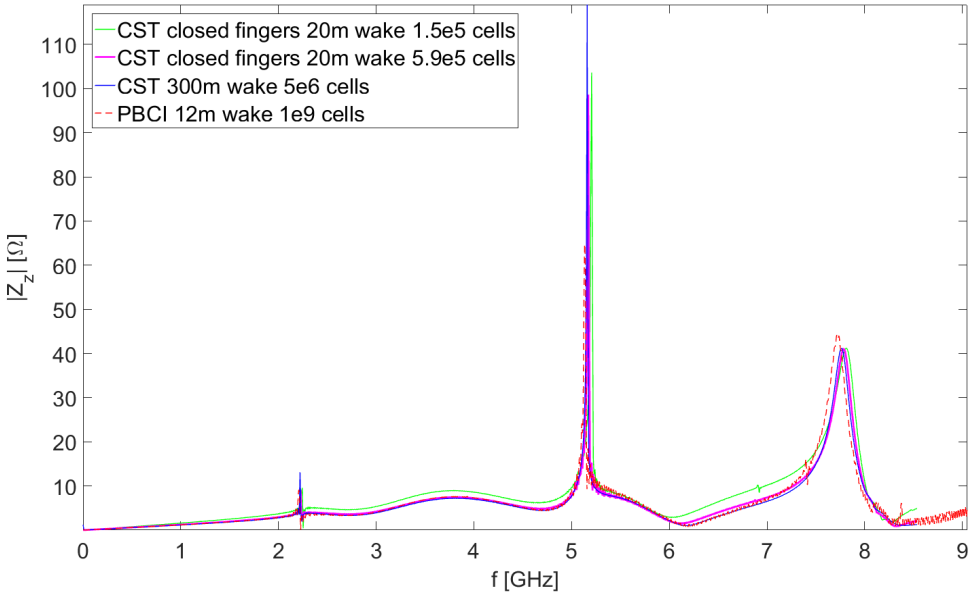


**Figure 5:** Comparison of PBCI and CST, also for the closed structure.

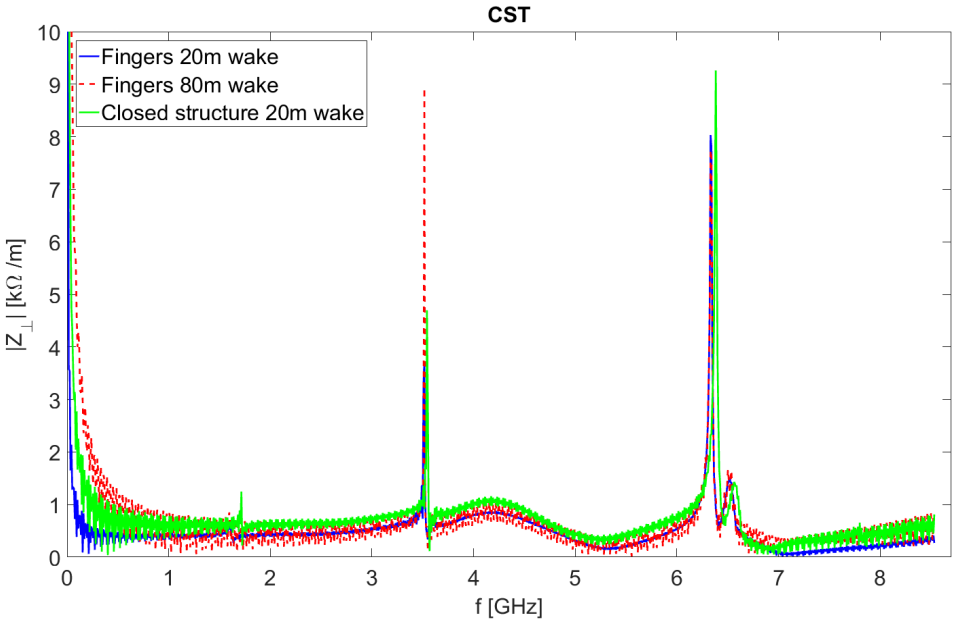


**Figure 6:** Dipolar transverse impedance magnitude.

### 2.7.5 **Frequency Domain Solver Example**

In FD, there is no direct advantage from the FIT diagonal material matrices, which favors the FEM on an unstructured mesh. However, in practice FIT is also used, since the structured mesh makes the implementation of Floquet boundary conditions simple [25]. Particularly in the absence of bulk materials, the Boundary Element Method (BEM) is also an attractive option in FD [26, 27]. The beam velocity and dispersive material data are just parameters in FD that can in principle be chosen arbitrarily. However, such parameters influence the condition number of the system matrix, which becomes an issue when a large System of Linear Equations (SLE) has to be solved for each frequency point.

We address an example for the FCC-hh [28] design study, i.e. a beam pipe design proposal (see Fig. 7), with the FEM code BeamImpedance2D [17]. The code solves the curl-curl equation

$$\nabla \times \underline{\mu}^{-1} \nabla \times \underline{\vec{E}} - \omega^2 \underline{\varepsilon}\,\underline{\vec{E}} = -i\omega \underline{\vec{J}}$$

for the electric field $\underline{\vec{E}} : R^2 \to C^3$, subject to the beam current density $\underline{\vec{J}}$ as the excitation. Note that $\underline{\vec{E}}$ and $\underline{\vec{J}}$ are not free of divergence due to the beam's charge. The permeability and permittivity are allowed to be complex, i.e. conductive, polarization and magnetization losses are taken care of. For the solution of the system Nedelec finite elements are used. Since those are (at lowest order) not capable of modelling the divergence of $\underline{\vec{E}}$, a Helmholtz split needs to be performed to calculate the (quasi) static fields from a complex potential separately (see [17]). Furthermore, the code allows using a Surface Impedance Boundary Condition (SIBC) to avoid meshing the extremely small skin depth at high frequency.

**Figure 7:** Proposed FCC beam pipe design (R. Kersevan) and GMSH mesh (T. Egenolf).

Figure 7 shows the proposed FCC-hh beam pipe design, where the green color indicates vacuum domains. The inner surface of the beam screen is covered by a copper layer of thickness 80 µm. In order to avoid meshing the material behind the copper, a two-layer surface impedance is used [29]. Figure 8 shows the transverse impedance of the structure, together with analytical results by ReWall [30] for circular pipes with the

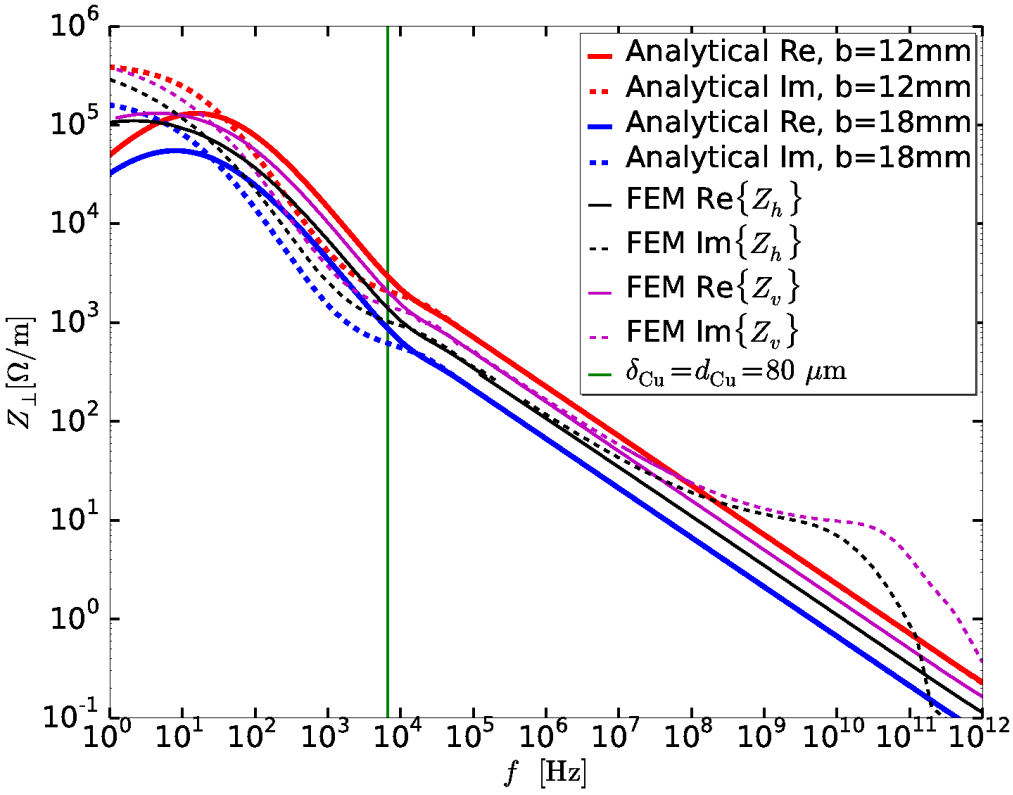


**Figure 8:** Transverse impedance of the FCC pipe.

the smaller and larger semi-axis radii 12mm and 18mm. As expected, the impedance curves for the real structure are between the two analytical curves and the horizontal is smaller than the vertical impedance due to the larger distance to the wall. The bump of the imaginary part at high frequency is a numerical artifact, due to improper cancelation of the electric and magnetic parts of the space charge impedance at the extremely high gamma=50000. At low frequency the discrepancies between the analytical and numerical results are due to different modelling of the structure. In ReWall the titanium behind the copper is considered with its thickness of 2mm and vacuum behind. The SIBC for BeamImpedance2D assumes infinite thickness of the titanium. However, this modeling discrepancy matters only for extremely low frequencies below 100Hz.

### 2.7.6 **Acknowledgements**

The authors wish to thank Benoit Salvant (CERN) for providing the CST model of the finger structure and Thilo Egenolf (TEMF) for modelling the FCC pipe.

### 2.7.7 **References**

1. V. G. Vaccaro, “Longitudinal Instability of a Coasting Beam above Transition, due to the action of Lumped Discontinuities,” CERN report ISR-RF/66-35, Tech. Rep., 1966.
2. V. Balakin, I. Koop, A. Novokhatsky, A. Skrinsky, and V. Smirnov, “Beam Dynamics of a Colliding Linear Electron-Positron Beam (VLEPP),” Tech. Rep. SLAC Trans 188, 1978.
3. T. Weiland, “Transient Electromagnetic Fields Excited by Bunches of Charged Particles in Cavities of Arbitrary Shape,” CERN ISR-TH/80-24, Tech. Rep., 1980.
4. K. Yee, IEEE Trans. Antennas Propag. 14 (1966) 302.
5. T. Weiland, Electronics and Communication 31 (1977) 116.
6. R. Courant, K. Friedrichs and H. Lewy, Über die partiellen Differenzengleichungen der mathematischen Physik, Math. Ann. 100 (1928) 32.
7. R. Gluckstern, Analytic methods for calculating coupling impedances, Cern Accelerator School, 2000.
8. A. Chao, Lecture Notes on Topics in Accelerator Physics, 2002
9. W.K.H. Panofsky and W.A. Wenzel, Rev. Sci. Instrum. 27 967, 1956.
10. O. Napoly, “The Wake Potentials from the Fields on the Cavity Boundary,” Particle Accelerators, vol. 36, pp. 15–23, 1991.
11. O. Napoly, Y. H. Chin, and B. Zotter, “A generalized method for calculating wake potentials,” Nucl. Instrum. Meth. Section A, vol. 334, no. 2-3, pp. 255–265, Oct. 1993.
12. T. Weiland, “Comment on Wake Field Computation in the Time Domain,” NIM, vol. 216, pp. 31–34, 1983
13. H. Henke and W. Bruns, “Calculation of Wake Potentials in general 3D structures,” in Proc. of EPAC, no. 8, 2006, pp. 2170–2172
14. X. Dong, E. Gjonaj, W. F. O. Mueller and T. Weiland, “Eignemode Expansion Method in the indirect calculation of wake potential in 3D structures” proc. of ICAP 2006 Chamonix, TUPPP31, 2006
15. I. Zagorodnov, “Indirect methods for wake potential integration,” Phys. Rev. ST Accel. Beams, 9, 102002 (2006).

16. M. Balk, R. Schuhmann and T. Weiland, Nucl. Instrum. Methods Phys. Res. A 558, 54, 2006.
17. U. Niedermayer, O. Boine-Frankenheim and H. De Gersem, "Space charge and resistive wall impedance computation in the frequency domain using the finite element method" Phys. Rev. ST Accel. Beams 18, 032001 (2015)
18. K. Bane and T. Weiland, "Wake force computation in the Time Domain for Long Structures", SLAC-PUB-3173, 1983
19. E. Gjonaj et al., ICFA Beam Dynamics Newsletter 45 (2008)
20. www.gdfidl.de
21. I. Zagorodnov and T. Weiland, Phys. Rev. ST Accel. Beams 8 (2005) 042001.
22. E.Gjonaj and T. Weiland, "Impedance Calculation. Time Domain", Handbook of Accelerator physics and Technology, 2nd edition edited by A.W. Chao, K.H. Mess, M. Tigner, F. Zimmermann, World Scientific (2013)
23. B. Salvant, private communication
24. www.cst.com
25. U. Niedermayer and O. Boine-Frankenheim, "Numerical Calculation of Beam Coupling Impedances in the Frequency Domain using FIT," in Proc. of ICAP 2012, Rostock, 2012.
26. K. Yokoya, Resistive Wall Impedance of Beam Pipes of General Cross Section, KEK Preprint 92-196 (1993).
27. A. Macridin, P. Spentzouris and J. Amundson, Phys. Rev. ST Accel. Beams 16 121001 (2013).
28. www.fcc.web.cern.ch
29. U. Niedermayer, O. Boine-Frankenheim and H. De Gersem, proc. of ICAP Shanghai, 2015
30. N. Mounet and E. Metral, Electromagnetic field created by a macroparticle in an infinitely long and axisymmetric multilayer beam pipe, CERN–BE–2009–039 (2009).